

# Time Dependent $B_s^0 - \overline{B}_s^0$ Mixing Using Inclusive and Semileptonic $\overline{B}$ Decays at SLD\*

The SLD Collaboration\*\*

Stanford Linear Accelerator Center,  
Stanford University, Stanford, CA 94309

## Abstract

We set a preliminary 95% C.L. exclusion on the oscillation frequency of  $B_s^0 - \overline{B}_s^0$  mixing using a sample of 400,000 hadronic  $Z^0$  decays collected by the SLD experiment at the SLC between 1996 and 1998. The analyses determine the  $b$ -hadron flavor at production by exploiting the large forward-backward asymmetry of polarized  $Z^0 \rightarrow b\overline{b}$  decays as well as information from the hemisphere opposite that of the reconstructed  $B$  decay. In one analysis,  $B$  decay vertices are reconstructed inclusively with a topological technique, and separation between  $B_s^0$  and  $\overline{B}_s^0$  decays exploits the  $B_s^0 \rightarrow D_s^-$  cascade charge structure. In the other analysis, semileptonic decays are selected and the  $B$  decay point is reconstructed by intersecting a lepton track with the trajectory of a topologically reconstructed  $D$  meson. The two analyses are combined with a third analysis described elsewhere to exclude the following values of the  $B_s^0 - \overline{B}_s^0$  mixing oscillation frequency:  $\Delta m_s < 7.6 \text{ ps}^{-1}$  and  $11.8 < \Delta m_s < 14.8 \text{ ps}^{-1}$  at the 95% confidence level.

*Paper Contributed to the XXXth International Conference on High Energy Physics  
(ICHEP 2000), 27 Jul – 2 Aug 2000, Osaka, Japan.*

---

\*Work supported in part by the Department of Energy contract DE-AC03-76SF00515.

# 1 Introduction

Transitions between  $B^0$  and  $\overline{B}^0$  mesons take place via second order weak interactions. In the Standard Model, a measurement of the oscillation frequency  $\Delta m_d$  for  $B_d^0-\overline{B}_d^0$  mixing determines, in principle, the value of the Cabibbo-Kobayashi-Maskawa matrix element  $|V_{td}|$  and constrains the Wolfenstein parameters  $\rho$  and (the CP-violating phase)  $\eta$ , which are currently poorly constrained. However, theoretical uncertainties in calculating hadronic matrix elements are large ( $\sim 20\%$  [1, 2]) and thus limit the current usefulness of precise  $\Delta m_d$  measurements. Some of these uncertainties cancel when one considers the ratio between  $\Delta m_d$  and  $\Delta m_s$ , leading to a reduced theoretical uncertainty ( $\sim 4-8\%$  [1, 2]). Thus, combining measurements of the oscillation frequency of both  $B_d^0-\overline{B}_d^0$  and  $B_s^0-\overline{B}_s^0$  mixing translates into a measurement of the ratio  $|V_{td}|/|V_{ts}|$  and provides a stronger constraint on the parameters  $\rho$  and  $\eta$ .

Experimentally, a measurement of the time dependence of  $B^0-\overline{B}^0$  mixing requires three ingredients: (i) the  $B$  decay proper time has to be reconstructed, (ii) the  $B$  flavor at production (initial state  $t = 0$ ) needs to be determined, as well as (iii) the  $B$  flavor at decay (final state  $t = t_{\text{decay}}$ ). At SLD, the time dependence of  $B_s^0-\overline{B}_s^0$  mixing has been studied using three different methods, two of which are described below. The third method (“D<sub>s</sub>+tracks”) is described elsewhere (see Ref. [3]). All methods use the same initial state flavor tag but they use different techniques to reconstruct the  $B$  decay and tag its final state flavor. The data consists of some 400,000 hadronic  $Z^0$  decays collected with the upgraded vertex detector (VXD3) between 1996 and 1998. The analyses exploit the large longitudinal polarization of the electron beam,  $P_e = (73.4 \pm 0.4)\%$  for 1996-98, to enhance the initial state tag.

## 2 Detector, Simulation and Event Selection

The components of the SLD detector relevant to this analysis are presented here. The Liquid Argon Calorimeter (LAC) was used for triggering, event shape measurement and electron identification. It provides excellent solid-angle coverage ( $|\cos\theta| < 0.84$  and  $0.82 < |\cos\theta| < 0.98$  in the barrel and endcap regions, respectively). The LAC is divided longitudinally into electromagnetic and hadronic sections. The energy resolution for electromagnetic showers is measured to be  $\sigma/E = 15\%/\sqrt{E(\text{GeV})}$ , whereas that for hadronic showers is estimated to be  $60\%/\sqrt{E(\text{GeV})}$ . The Warm Iron Calorimeter (WIC) provides efficient muon identification for  $|\cos\theta| < 0.60$ . Tracking is provided by the Central Drift Chamber (CDC)[4] for charged track reconstruction and momentum measurement and the CCD pixel Vertex Detector (VXD)[5] for precise position measurements near the interaction point. Aside from the WIC, these systems are immersed in the 0.6 T field of the SLD solenoid. Charged tracks reconstructed in the CDC are linked with pixel clusters in the VXD by extrapolating each track and selecting the best set of associated clusters[4]. The track impact parameter resolutions at high momenta are  $7.8\ \mu\text{m}$  and  $9.7\ \mu\text{m}$  in the  $r\phi$  and  $rz$  projections respectively ( $z$  points along the beam direction), while multiple scattering contributions are  $33\ \mu\text{m}/(p \sin^{3/2}\theta)$  in both projections (where the momentum  $p$  is expressed in GeV/c).

The centroid of the micron-sized SLC Interaction Point (IP) in the  $r\phi$  plane is reconstructed with a measured precision of  $\sigma_{IP} = (4 \pm 2) \mu\text{m}$  using tracks in sets of  $\sim 30$  sequential hadronic  $Z^0$  decays. The median  $z$  position of tracks at their point of closest approach to the IP in the  $r\phi$  plane is used to determine the  $z$  position of the  $Z^0$  primary vertex on an event-by-event basis. A precision of  $\sim 20 \mu\text{m}$  on this quantity is estimated using the  $Z^0 \rightarrow b\bar{b}$  Monte Carlo (MC) simulation.

The simulated  $Z^0 \rightarrow q\bar{q}$  events are generated using JETSET 7.4 [6]. The  $B$  meson decays are simulated using the CLEO  $B$  decay model [7] tuned to reproduce the spectra and multiplicities of charmed hadrons, pions, kaons, protons and leptons as measured at the  $\Upsilon(4S)$  by ARGUS and CLEO [8]. Semileptonic decays of  $B$  mesons follow the ISGW model [9] including 23%  $D^{**}$  production. The branching fractions of the charmed hadrons are tuned to the existing measurements [10]. The lifetimes of  $B$  mesons and  $b$ -baryons are chosen to be  $\tau_{B^+} = 1.656$  ps,  $\tau_{B^0} = 1.562$  ps,  $\tau_{B_s^0} = 1.464$  ps, and  $\tau_{\Lambda_b} = 1.208$  ps, according to recent world averages [11]. The  $b$ -quark fragmentation follows the Peterson *et al.* parameterization [12]. Finally, the SLD detector is simulated using GEANT 3.21 [13].

Hadronic  $Z^0$  event selection requires at least 7 CDC tracks which pass within 5 cm of the IP in  $z$  at the point of closest approach to the beam and which have momentum transverse to the beam direction  $p_{\perp} > 200$  MeV/ $c$ . The sum of the energy of the charged tracks passing these cuts must be greater than 18 GeV. These requirements remove background from  $Z^0 \rightarrow l^+l^-$  events and two-photon interactions. In addition, the thrust axis determined from energy clusters in the calorimeter must have  $|\cos\theta_T| < 0.85$ , within the acceptance of the vertex detector. These requirements yield a sample of  $\sim 311,000$  hadronic  $Z^0$  decays.

Good quality tracks used for vertex finding must have at least two associated VXD hits and  $p_{\perp} > 250$  MeV/ $c$ . Additional requirements are that the tracks have either three or more VXD hits or else satisfy the following criteria: (i) have a CDC hit at a radius  $< 50$  cm, (ii) have  $\geq 23$  hits to insure that the lever arm provided by the CDC is appreciable, (iii) extrapolate to within 1 cm of the IP in  $r\phi$  and within 1.5 cm in  $z$  to eliminate tracks which arise from interaction with the detector material, (iv) have a  $\chi^2/\text{d.o.f.} < 8$  for both the CDC portion of the track and the combined VXD-CDC track.

Tracks reconstructed in the vertex detector but unsuccessfully tracked in the drift chamber are also used in the analyses. Such “VXD-only” tracks are constructed from hits in all three of the vertex detector layers and are used primarily to improve the overall vertex charge reconstruction.

Both analyses make use of the inclusive topological vertexing technique [14] developed for  $B$  lifetime [15] and  $R_b$  [16] analyses to tag and reconstruct  $b$ -hadron decays. The  $b$  purity of the sample is increased by reconstructing the vertex mass  $M$ , which includes a partial correction for missing decay products (see Ref. [4]). This inclusive vertexing technique has been adapted for semileptonic decays to reconstruct the  $D$  decay topology (see below).

### 3 Initial State Flavor Tagging

The large forward-backward asymmetry for polarized  $Z^0 \rightarrow b\bar{b}$  decays is used as a tag of the initial state flavor. The polarized forward-backward asymmetry  $\tilde{A}_{FB}$  can be described by

$$\tilde{A}_{FB}(\cos \theta_T) = 2A_b \frac{A_e - P_e}{1 - A_e P_e} \frac{\cos \theta_T}{1 + \cos^2 \theta_T} , \quad (1)$$

where  $A_b = 0.935$  and  $A_e = 0.150$  (Standard Model values),  $P_e$  is the electron beam longitudinal polarization, and  $\theta_T$  is the angle between the thrust axis and the electron beam direction (the thrust axis is signed such that it points in the same hemisphere as the reconstructed  $B$  vertex). Thus, left- (right-)polarized electrons tag  $b$  ( $\bar{b}$ ) quarks in the forward hemisphere, and  $\bar{b}$  ( $b$ ) quarks in the backward hemisphere. Averaged over our acceptance, this yields an average correct tag probability of 0.74 for an average electron polarization  $P_e = 73\%$ . The probability for correctly tagging a  $b$  quark at production is expressed as

$$P_A(\cos \theta_T) = \frac{1 + \tilde{A}_{FB}(\cos \theta_T)}{2} . \quad (2)$$

A jet charge technique is used in addition to the polarized forward-backward asymmetry. For this tag, tracks in the hemisphere opposite that of the reconstructed vertex are selected. These tracks are required to have momentum transverse to the beam axis  $p_\perp > 0.15$  GeV/c, total momentum  $p < 50$  GeV/c, impact parameter in the plane perpendicular to the beam axis  $\delta < 2$  cm, distance between the primary vertex and the track at the point of closest approach along the beam axis  $\Delta z < 10$  cm, and  $|\cos \theta| < 0.90$ . With these tracks, an opposite hemisphere momentum-weighted track charge is defined as

$$Q_{opp} = \sum_i q_i \left| \vec{p}_i \cdot \hat{T} \right|^\kappa , \quad (3)$$

where  $q_i$  is the electric charge of track  $i$ ,  $\vec{p}_i$  its momentum vector,  $\hat{T}$  is the thrust axis direction, and  $\kappa$  is a coefficient chosen to be 0.5 to maximize the separation between  $b$  and  $\bar{b}$  quarks. The probability for correctly tagging a  $b$  quark in the initial state of the vertex hemisphere can be parameterized as

$$P_Q(Q_{opp}) = \frac{1}{1 + e^{\alpha Q_{opp}}} , \quad (4)$$

where the coefficient  $\alpha = -0.27$ , as determined using the Monte Carlo simulation. This technique yields an average correct tag probability of 0.66 and is independent of the polarized forward-backward asymmetry tag.

Finally, the tag is further enhanced by the addition of other flavor-sensitive quantities from the hemisphere opposite that of the selected vertex. For this purpose, the inclusive topological vertexing technique mentioned earlier is used. The sensitive variables are: the total track charge and charge dipole of a topologically reconstructed vertex, the charge of a kaon identified in the Cherenkov Ring Imaging Detector, and the charge of a lepton with high transverse momentum with respect to the direction of the nearest jet. The addition of these tags improves the average correct tag probability by about 0.03.

The various tags are combined, taking correlations into account, to form an overall initial state tag characterized by a  $b$ -quark probability  $P_i$ . The average correct tag probability is 0.75 for the lepton+D and 0.77 for the charge dipole analyses with 100% efficiency. Fig. 1 shows the  $P_i$  distributions for data and Monte Carlo in the charge dipole analysis (see below for a description of the analysis), and also indicates the clear separation between  $b$  and  $\bar{b}$  quarks.

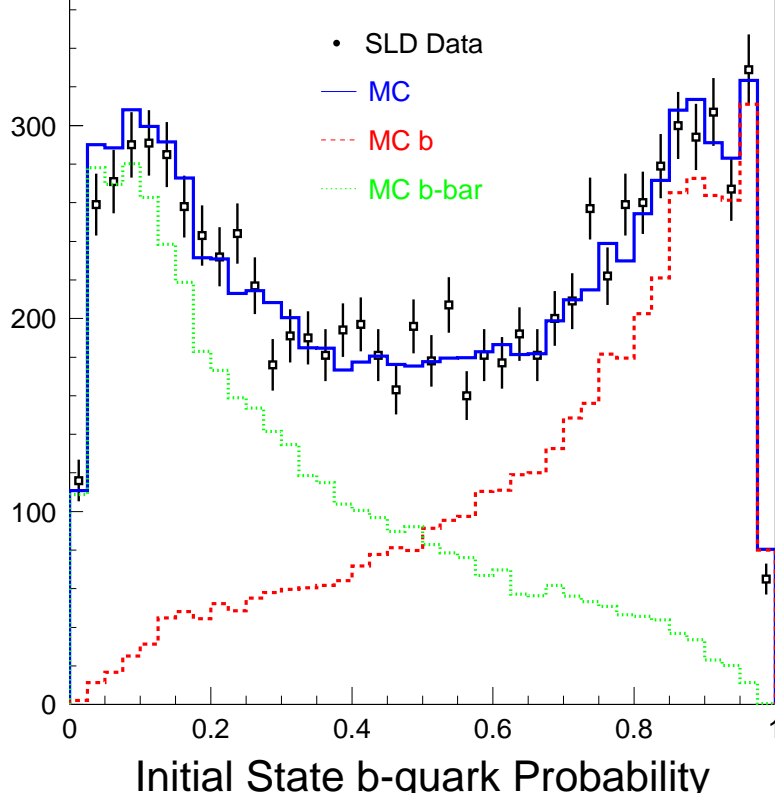


Figure 1: *Distribution of the computed initial state  $b$ -quark probability for data (points) and Monte Carlo (histograms) showing the  $b$  and  $\bar{b}$  components for the events selected in the charge dipole analysis.*

## 4 Lepton+D Analysis

The lepton+“D” analysis aims at reconstructing the  $B$  and  $D$  vertex topologies of semileptonic  $B$  decays. It proceeds by first selecting event hemispheres containing an identified lepton ( $e$  or  $\mu$ ) with  $|\cos \theta| < 0.7$ . Then, a  $D$  vertex candidate is reconstructed using the inclusive topological technique described earlier. If multiple displaced vertices are found in the same hemisphere, the vertex with the largest invariant mass is chosen to be the  $D$  vertex candidate. A resultant  $D$  “track” is created using the  $D$  vertex location and the parameters of all tracks attached to it. Furthermore, the  $D$  track error matrix is corrected

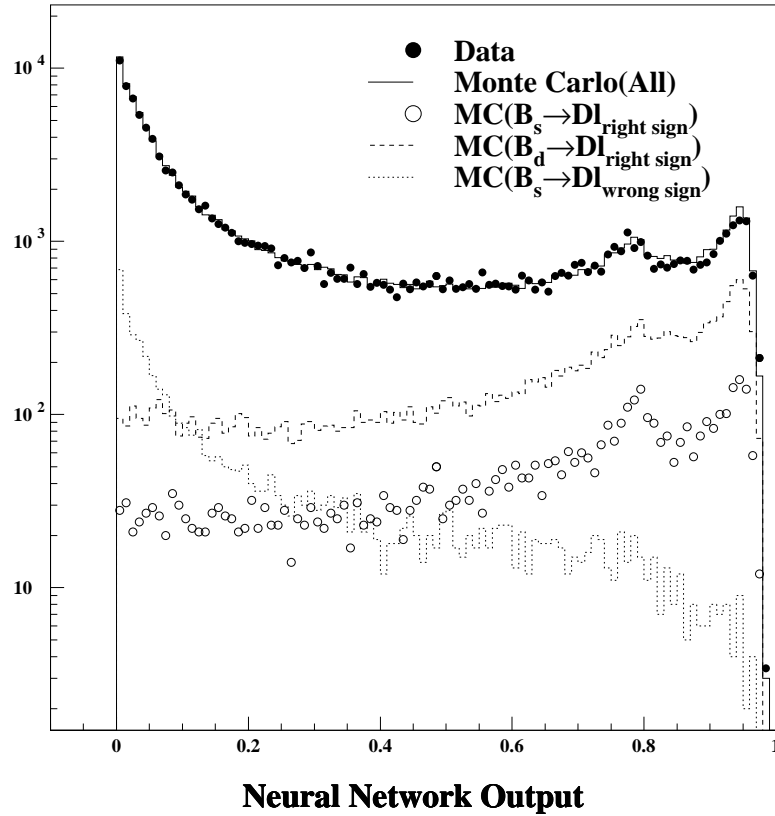


Figure 2: *Distribution of neural network output variable for data (solid points) and Monte Carlo (solid histogram). Also shown are the Monte Carlo distributions for  $B_s^0$  right-sign leptons (open circles),  $B_d^0$  right-sign leptons (dashed histogram) and  $B_s^0$  wrong-sign leptons (dotted histogram).*

to take into account the fact that the  $D$  decay is not fully reconstructed. Finally, the  $B$  decay vertex is reconstructed by intersecting the lepton and  $D$  tracks.

A neural network is used to clean up the  $D$  vertex candidates and reduce the contamination from cascade ( $b \rightarrow c \rightarrow l$ ) charm semileptonic decays. The Jetnet neural network package is used with 6 inputs and 12 hidden nodes. The inputs are the transverse momentum of the lepton with respect to the  $B$  vertex direction (vector stretching from the IP to the  $B$  vertex), the  $B$  decay length (magnitude of that vector), the transverse momentum of the lepton with respect to the  $D$  vertex direction (vector stretching from the  $B$  vertex to the  $D$  vertex), the mass  $M$  of the charged tracks associated with the  $B$  decay and the distance of closest approach of the lepton to the  $B$  vertex. A distribution of the neural network output is shown in Fig. 2. A minimum cut of 0.65 is applied on the neural network output.

For this analysis, only vertices with positive reconstructed decay length are selected. To enhance the fraction of  $B_s^0$  decays, the sum of lepton +  $D$  vertex track charges is required to be  $Q = 0$ . This enhances the  $B_s^0$  fraction to 16.4% of all  $b$  hadrons in the  $Z^0 \rightarrow b\bar{b}$  MC (the  $B_s^0$  production fraction in the  $Z^0 \rightarrow b\bar{b}$  MC is 10.0%). The  $udsc$

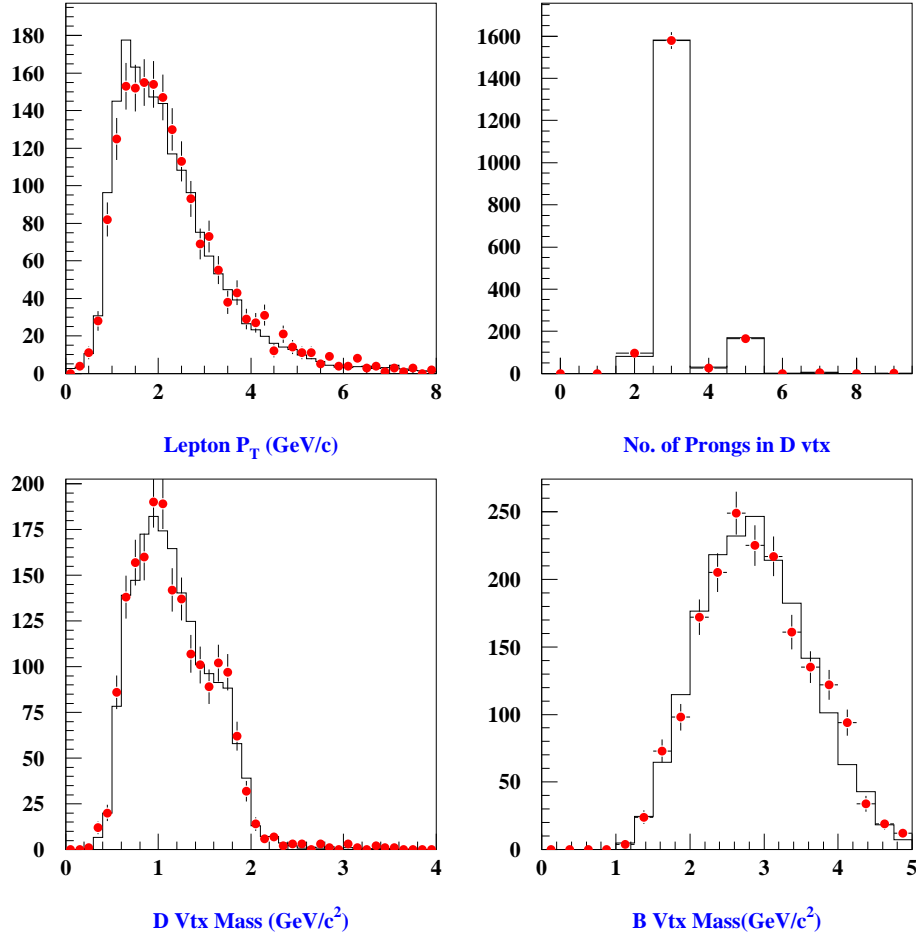


Figure 3: *Distributions of lepton momentum transverse to the  $D$  vertex trajectory,  $D$  vertex track multiplicity,  $D$  vertex mass and lepton+ $D$  vertex mass for data (points) and Monte Carlo (histograms).*

contamination is 0.5% in the final sample.

The  $B_s^0$  fraction is further enhanced by using the Cherenkov Ring Imaging Detector to identify kaon candidates among the  $D$  vertex tracks. For the subsample containing a lepton-kaon pair with opposite charge, the  $B_s^0$  fraction increases to 38.5% and the  $udsc$  contamination remains at 0.5%, as determined from MC.

A sample of 2087 decays is thus obtained in the 1996-98 data. Various comparisons between data and Monte Carlo simulation were performed which showed good agreement. For example, Fig. 3 shows the distributions of lepton momentum transverse to the  $D$  vertex trajectory,  $D$  vertex track multiplicity, and invariant mass of all tracks in the  $D$  vertex and (assuming all tracks are pions) as well as in both  $B$  and  $D$  vertices.

A powerful check of the analysis and the purity of the final state tag is the polarization-dependent forward-backward asymmetry shown in Fig. 4. A clear asymmetry is observed, in reasonable agreement with the Monte Carlo, indicating that the

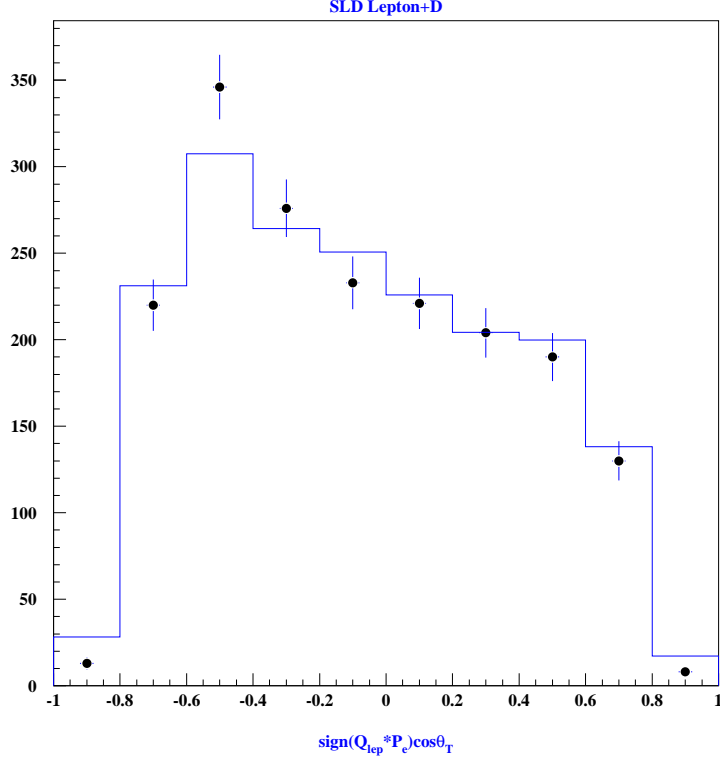


Figure 4: *Distribution of  $\cos \theta$  for the thrust axis direction signed by the product  $(Q_{\text{lepton}} \times P_e)$  for data (points) and Monte Carlo (histogram).*

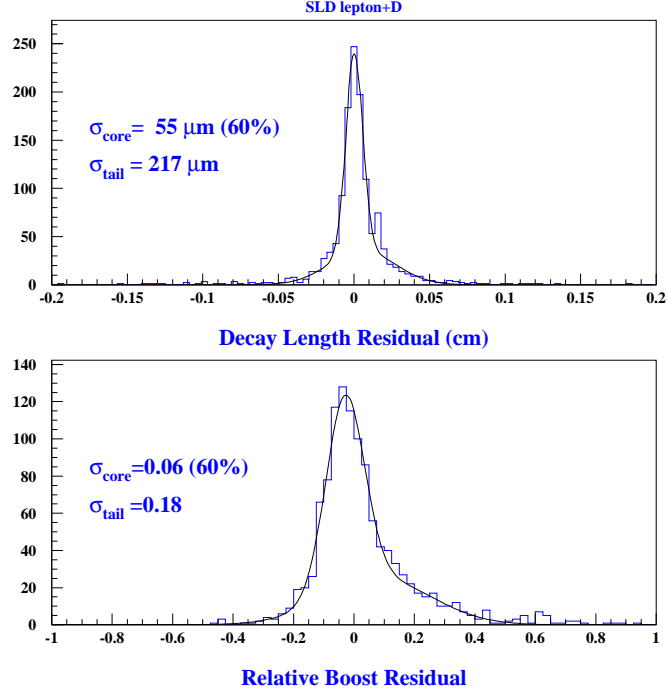


Figure 5: *Distributions of the decay length and relative boost residuals for  $B_s^0$  ( $b \rightarrow l$ ) decays in the simulation.*



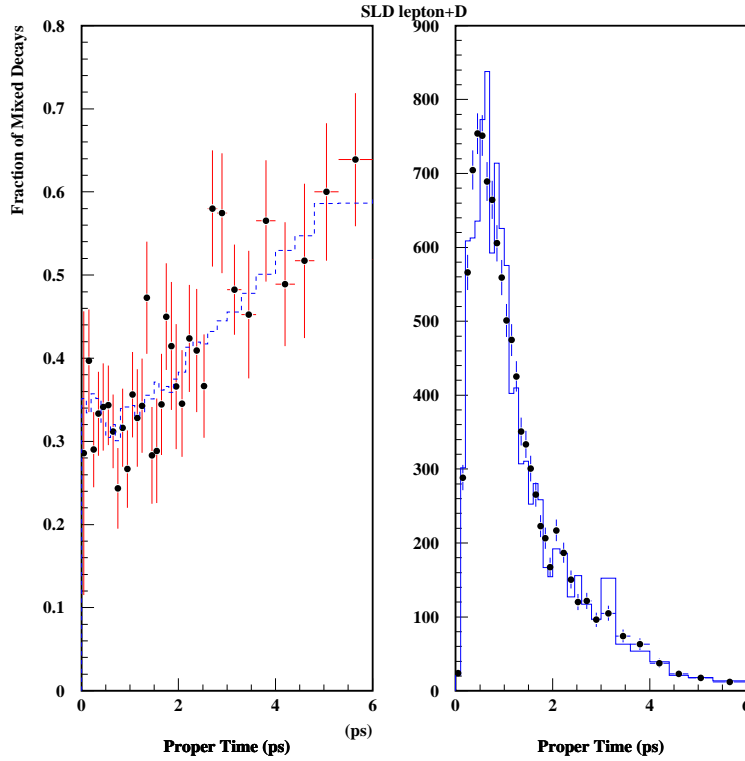


Figure 6: *Distributions of the fraction of decays tagged as “mixed” as a function of reconstructed proper time (left) and reconstructed proper time (right) for the data (points) and the likelihood function (histograms).*

final state tag purity is adequately modeled in the simulation.

The study of the time dependence of  $B_s^0\text{--}\overline{B}_s^0$  mixing requires a precise determination of the  $B$  decay proper time  $t = L/(\gamma\beta c)$ , where  $L$  is the reconstructed decay length (distance between the IP and the  $B$  vertex) and  $\gamma\beta = p_B/m_B$  is computed from the estimated  $B$  momentum  $p_B$  and the known mass of the  $B$  meson,  $m_B$ . Reconstruction of the  $b$ -hadron boost uses both tracking and calorimeter information. A description of the reconstruction algorithm may be found in Ref. [17]. The overall performance of the decay length and boost measurements for  $B_s^0$  decays proceeding via the direct ( $b \rightarrow l$ ) transition is shown in Fig. 5. The proper time distribution is shown in Fig. 6.

The final state  $B^0$  or  $\overline{B}^0$  flavor is tagged by the sign of the lepton charge. Each decay is assigned a final state  $b$ -quark probability  $P_f$ , defined such that  $P_f > 0.5$  ( $< 0.5$ ) corresponds to a negatively (positively) charged lepton which then tags the decay as  $\overline{B}$  ( $B$ ). The magnitude of the correct tag probability depends on the sample composition as well as on the lepton  $p_T$ . The lepton sources in selected  $B_s^0$  decays are as follows: 94.8% ( $b \rightarrow l^-$ ), 2.6% ( $b \rightarrow c \rightarrow l^+$ ), 1.4% ( $b \rightarrow \bar{c} \rightarrow l^-$ ), 0.6% ( $b \rightarrow X^-$ ) (right-sign misidentified lepton), and 0.6% ( $b \rightarrow X^+$ ) (wrong-sign misidentified lepton). The final state correct tag probability is thus 0.968. Further enhancement of the tag is achieved by taking into account the strong  $p_T$  dependence of the various lepton source fractions.

## 4.1 Likelihood Function

The search for the time dependence of  $B_s^0 - \overline{B}_s^0$  mixing is carried out with a likelihood analysis which includes the effect of detector smearing, mistag of both initial and final states, selection efficiencies and the dependence on the oscillation frequency  $\Delta m_s$ . The probability that a meson created as a  $B_s^0$  ( $\overline{B}_s^0$ ) will decay as a  $B_s^0$  ( $\overline{B}_s^0$ ) after proper time  $t$  can be written as

$$P_u(t) = \frac{\Gamma}{2} e^{-\Gamma t} [1 + \cos(\Delta m_s t)] , \quad (5)$$

where  $\Delta m_s$  is the mass difference between the mass eigenstates,  $\Gamma$  is the average decay width of the two states and  $P_u$  denotes the probability to remain ‘unmixed’. The effects of CP violation are assumed to be small and are neglected. Similarly, the probability that the same initial state will ‘mix’ and decay as its antiparticle is

$$P_m(t) = \frac{\Gamma}{2} e^{-\Gamma t} [1 - \cos(\Delta m_s t)] . \quad (6)$$

Decays are tagged as mixed or unmixed if the product  $(P_i - 0.5) \times (P_f - 0.5)$  is smaller or greater than 0, respectively. The probability for a decay to be in the mixed sample is expressed as:

$$\begin{aligned} \mathcal{P}_{mixed}(t, \Delta m_s) = & f_u \frac{e^{-t/\tau_u}}{\tau_u} \left[ w^I (g_u^{dl} + g_u^{cr} + g_u^{xr}) + (1 - w^I) (g_u^{cw} + g_u^{xw}) \right] \\ & + \frac{f_d}{2} \frac{e^{-t/\tau_d}}{\tau_d} \left[ (g_d^{dl} + g_d^{cr} + g_d^{xr}) (1 + [2w^I - 1] \cos \Delta m_d t) + (g_d^{cw} + g_d^{xw}) (1 - [2w^I - 1] \cos \Delta m_d t) \right] \\ & + \frac{f_s}{2} \frac{e^{-t/\tau_s}}{\tau_s} \left[ (g_s^{dl} + g_s^{cr} + g_s^{xr}) (1 + [2w^I - 1] \cos \Delta m_s t) + (g_s^{cw} + g_s^{xw}) (1 - [2w^I - 1] \cos \Delta m_s t) \right] \\ & + f_{baryon} \frac{e^{-t/\tau_{baryon}}}{\tau_{baryon}} \left[ w^I (g_{baryon}^{dl} + g_{baryon}^{cr} + g_{baryon}^{xr}) + (1 - w^I) (g_{baryon}^{cw} + g_{baryon}^{xw}) \right] \\ & + \frac{f_{udsc}}{2} F_{udsc}(t), \end{aligned} \quad (7)$$

where  $f_j$  represents the fraction of each  $b$ -hadron type and background ( $j = u, d, s, \Lambda$ , and  $udsc$  correspond to  $B^+$ ,  $B_d^0$ ,  $B_s^0$ ,  $b$ -baryon, and  $udsc$  background),  $\tau_j$  is the lifetime for  $b$  hadrons of type  $j$ ,  $w^I$  is the initial state mistag probability,  $g_j^{dl}$ ,  $g_j^{cr}$  and  $g_j^{xr}$  are the fractions of right-sign ( $b \rightarrow l^-$ ), ( $b \rightarrow \bar{c} \rightarrow l^-$ ) and ( $b \rightarrow X^-$ ) leptons, respectively,  $g_j^{cw}$  and  $g_j^{xw}$  are the fractions of wrong-sign ( $b \rightarrow c \rightarrow l^+$ ) and ( $b \rightarrow X^+$ ) leptons, respectively, and  $F_{udsc}(t)$  is a function describing the proper time distribution of the  $udsc$  background (a sum of two exponentials is used). A similar expression for the probability  $\mathcal{P}_{unmixed}$  to observe a decay tagged as unmixed is obtained by replacing the mistag rate  $w^I$  by  $1 - w^I$ .

Detector and vertex selection effects are introduced by convoluting the above probability functions with a proper time resolution function  $\mathcal{R}(T, t)$  and a time-dependent efficiency function  $\varepsilon(t)$ :

$$P_{mixed}(T, \Delta m_s) = \int_0^\infty \mathcal{P}_{mixed}(t, \Delta m_s) \mathcal{R}(T, t) \varepsilon(t) dt , \quad (8)$$

where  $t$  is the “true” time and  $T$  is the reconstructed time. Again, a similar expression applies to the unmixed probability  $P_{unmixed}$ . The resolution function is parameterized by the sum of four Gaussians:

$$\mathcal{R}(T, t) = \sum_{i=1}^2 \sum_{j=1}^2 f_{ij} \frac{1}{\sigma_{ij}(t)\sqrt{2\pi}} e^{-\frac{1}{2}\left(\frac{T-t}{\sigma_{ij}(t)}\right)^2}, \quad (9)$$

where the index  $i = 1$  ( $i = 2$ ) corresponds to the core (tail) component of the decay length resolution  $\sigma_{Li}$ , the index  $j = 1$  ( $j = 2$ ) similarly corresponds to the core (tail) component of the relative boost resolution  $\sigma_{\gamma\beta j}/\gamma\beta$ . The various fractions are  $f_{11} = 0.36$ ,  $f_{12} = f_{21} = 0.24$ , and  $f_{22} = 0.16$ . The proper time resolution  $\sigma_{ij}(t)$  is a function of proper time that depends on the measured boost  $\gamma\beta$ , its resolution and the decay length resolution:

$$\sigma_{ij}(t) = \left[ \left( \frac{\sigma_{Li}}{\gamma\beta c} \right)^2 + \left( t \frac{\sigma_{\gamma\beta j}}{\gamma\beta} \right)^2 \right]^{1/2}. \quad (10)$$

For each decay, the resolution  $\sigma_L$  is computed from the vertex fit and IP position measurement errors, with a scale factor determined using the MC simulation (the scale factor is introduced mostly to account for the fact that the analysis does not attempt to fully reconstruct the  $D$  meson decay). The relative boost residual  $\sigma_{\gamma\beta}/\gamma\beta$  is parameterized as a function of the lepton +  $D$  vertex total track energy, with parameters extracted from the MC simulation. Similarly, the efficiency  $\varepsilon(t)$  is parameterized using the MC simulation. All parameterizations are performed separately for each  $b$ -hadron type. For example, the efficiency for  $B_s^0$  decays is given by

$$\varepsilon(t) = a \frac{1 - e^{bt}}{1 + e^{bt}} + c, \quad (11)$$

with  $a = 0.148$ ,  $b = -5.7$ , and  $c = 0.0072$ . Furthermore,  $\sigma_L$  and  $\sigma_{\gamma\beta}$  resolutions are handled separately for the main lepton sources ( $b \rightarrow l$ ), ( $b \rightarrow c(\bar{c}) \rightarrow l$ ) and ( $b \rightarrow X$ ). As a consequence, different resolution functions are used for the different sources and the expressions for  $P_{mixed}$  and  $P_{unmixed}$  are modified accordingly.

The likelihood function is constructed from the calculated probabilities for events tagged as mixed and unmixed. The total likelihood for the sample is given by

$$\mathcal{L} = \prod_{i=1}^{\#mixed} P_{mixed} \prod_{j=1}^{\#unmixed} P_{unmixed}. \quad (12)$$

## 4.2 Oscillation Analysis

The study of the time dependence of  $B_s^0 - \overline{B}_s^0$  mixing is carried out using the amplitude method described in Ref. [18]. Instead of fitting for  $\Delta m_s$  directly, the analysis is performed at fixed values of  $\Delta m_s$  and a fit to the amplitude  $A$  of the oscillation is performed, i.e. in the expression for the mixed and unmixed probabilities, one replaces  $[1 \pm \cos(\Delta m_s t)]$  with  $[1 \pm A \cos(\Delta m_s t)]$ . This method is similar to Fourier transform analysis and has the advantage of facilitating the combination of results from different analyses and different experiments.

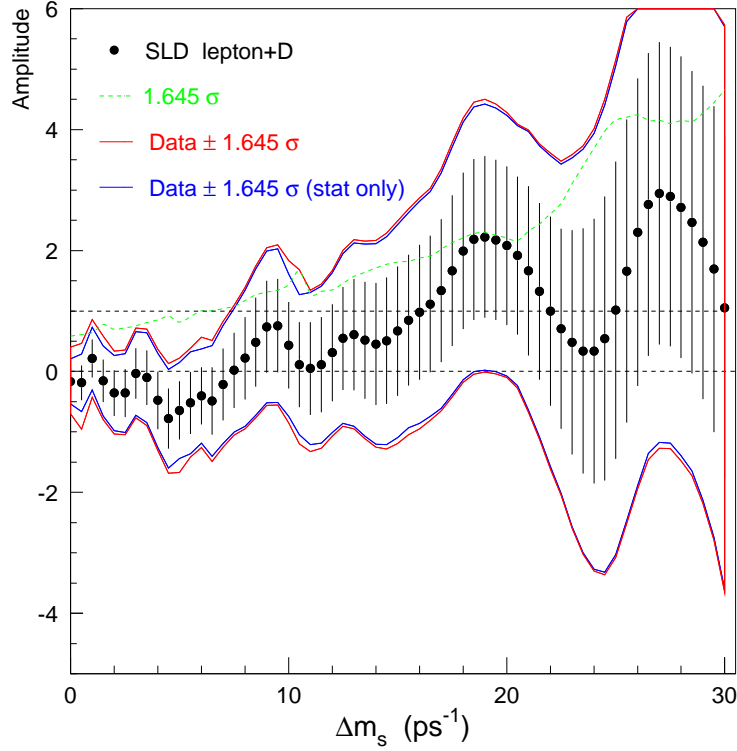


Figure 7: *Measured amplitude as a function of  $\Delta m_s$  in the lepton+D analysis.*

The measured amplitude for the lepton+D analysis is shown as a function of  $\Delta m_s$  in Fig. 7. The measured values are consistent with  $A = 0$  for the whole range of  $\Delta m_s$  up to  $30 \text{ ps}^{-1}$  and no evidence is found for a preferred mixing frequency.

Systematic uncertainties have been computed following Ref. [18] and are summarized in Table 1 for several  $\Delta m_s$  values. Uncertainties in the sample composition are estimated by varying the fraction of  $udsc$  background by  $\pm 20\%$  and the production fractions of  $B_s^0$  and  $b$ -baryons according to  $0.100 \pm 0.012$  and  $0.099 \pm 0.017$ , respectively [11]. Other physics modeling uncertainties are  $\tau(B^+) = 1.656 \pm 0.025 \text{ ps}$ ,  $\tau(B_d^0) = 1.562 \pm 0.029 \text{ ps}$ ,  $\tau(B_s^0) = 1.464 \pm 0.057 \text{ ps}$ ,  $\tau(\Lambda_b) = 1.208 \pm 0.051 \text{ ps}$ , and  $\Delta m_d = 0.480 \pm 0.020 \text{ ps}^{-1}$ . Uncertainties in the modeling of the detector include  $\pm 10\%$  and  $\pm 20\%$  variations in decay length and boost resolutions, respectively. Initial state tag uncertainties are estimated by varying the correct tag probability by  $\pm 0.02$  (i.e., a  $\pm 10\%$  variation of the mistag rate), corresponding to the expected contribution from uncertainties in the measured electron beam polarization, the value of  $A_b$ , and the self-calibrated jet charge analyzing power. Final state tag uncertainties include a  $\pm 15\%$  variation in the lepton misidentification rate, as well as the effect of uncertainties in the branching ratios  $\mathcal{B}(b \rightarrow l) = 0.112 \pm 0.002$ ,  $\mathcal{B}(b \rightarrow \bar{c} \rightarrow l) = 0.016 \pm 0.004$ , and  $\mathcal{B}(b \rightarrow c \rightarrow l) = 0.080 \pm 0.004$ . The dominant uncertainty is the  $B_s^0$  production fraction in  $Z^0 \rightarrow b\bar{b}$  events.

Table 1: Measured values of the oscillation amplitude  $A$  with a breakdown of the main systematic uncertainties for several  $\Delta m_s$  values in the lepton+D analysis.

$\Delta m_s$	5 ps <sup>-1</sup>	10 ps <sup>-1</sup>	15 ps <sup>-1</sup>	20 ps <sup>-1</sup>
Measured amplitude $A$	-0.644	0.433	0.668	2.080
$\sigma_A^{stat}$	$\pm 0.482$	$\pm 0.714$	$\pm 1.070$	$\pm 1.310$
$\sigma_A^{syst}$	+0.113 -0.442	+0.503 -0.253	+0.249 -0.389	+0.292 -0.168
$f_s = \mathcal{B}(b \rightarrow B_s^0)$	-0.134 +0.094	-0.076 +0.296	-0.169 +0.221	-0.027 +0.202
$f_\Lambda = \mathcal{B}(b \rightarrow b\text{-baryon})$	+0.047 -0.051	+0.065 -0.096	+0.042 -0.041	+0.025 -0.027
decay length resolution	+0.003 -0.002	-0.007 +0.008	+0.028 -0.033	+0.005 -0.044
boost resolution	-0.162 -0.040	+0.362 -0.113	+0.012 -0.327	+0.206 -0.138
$B_s^0$ lifetime	+0.033 -0.061	+0.049 -0.176	+0.033 -0.034	+0.002 -0.036
$\Delta m_d$	-0.093 -0.008	+0.010 -0.028	+0.000 -0.000	+0.004 -0.005
initial state tag	+0.014 -0.226	-0.001 +0.003	-0.022 +0.029	-0.025 +0.017
$\mathcal{B}(b \rightarrow l), \mathcal{B}(b \rightarrow \bar{c} \rightarrow l), \mathcal{B}(b \rightarrow c \rightarrow l)$	+0.012 -0.195	+0.163 -0.000	+0.064 -0.070	+0.019 -0.024
lepton misidentification	+0.008 -0.010	+0.015 -0.025	-0.005 +0.005	+0.000 -0.004

## 5 Vertex Charge Dipole Analysis

The charge dipole analysis aims at selecting decays with distinct  $B$  and  $D$  vertices and tags the  $B^0$  or  $\overline{B}^0$  decay flavor based on the charge difference between them. This analysis technique was first developed by SLD and relies extensively on the excellent resolution of the vertex detector.

In the following, we first describe the algorithm used to identify primary, secondary and tertiary vertices, then discuss details of the  $B_s^0\text{-}\overline{B}_s^0$  mixing analysis.

### 5.1 Ghost Track Algorithm

The  $B$  decay flavor tag with the charge dipole relies on the kinematic fact that the boost of the  $B$  decay system carries the cascade charm decay downstream from the  $B$  decay vertex. Monte Carlo studies show that in  $B$  decays producing a single  $D$  meson the cascade  $D$  decays on average 4200  $\mu\text{m}$  from the IP, while the intermediate  $B$  vertex is displaced on average only 46  $\mu\text{m}$  transversely from the line joining the IP to the  $D$  decay vertex. This kinematic stretching of the  $B$  decay chain into an approximately straight line is exploited by the ghost track algorithm. This new algorithm has two stages and operates on a given set of selected tracks in a jet or hemisphere. First, the best estimate of the straight line from the IP directed along the  $B$  decay chain is found. This line is promoted to the status of a track by assigning it a finite width. This new track, regarded as the resurrected image of the deceased  $B$  hadron, is called the “ghost” track. Secondly, the selected tracks are vertexed with the ghost track and the IP to build up the decay chain along the ghost direction. Both stages are now described in more detail.

Given a set of tracks in a hadronic jet or hemisphere a new track G is created with the properties that it is a straight line from the IP directed along the jet or thrust axis and has a constant resolution width of  $25\mu\text{m}$  in both  $r\phi$  and  $rz$ . For each track  $i$  a vertex is formed with track G and the vertex location  $\mathbf{r}_i$ , fit  $\chi_i^2$  and  $L_i$  are determined ( $L_i$  is the longitudinal displacement from the IP of  $\mathbf{r}_i$  projected onto the direction of track G). This is calculated for each of the tracks and the summed  $\chi^2$  is formed:

$$\chi_S^2 = \sum_i \begin{cases} \chi_i^2 & L_i \geq 0.0 \\ (2\chi_{0i}^2 - \chi_i^2) & L_i < 0.0 \end{cases} \quad (13)$$

where  $\chi_{0i}^2$  is the  $\chi_i^2$  of track  $i$  to track G determined at  $L_i = 0$  rather than at the best fit vertex location. The aim is to construct this quantity,  $\chi_S^2$ , such that when the direction of G is varied the minimum of  $\chi_S^2$  provides the best estimate of the  $B$  decay direction. If the initial direction is a relatively long way from the  $B$  line of flight, some or all of the decay tracks may vertex with G with a negative value of  $L_i$ . In this case the  $2\chi_{0i}^2 - \chi_i^2$  term above helps to push track G towards the  $B$  flight path as  $\chi_S^2$  is minimized. This first minimization using equation 13 is designed for this purpose. (Note that the contribution of each track as  $\chi_S^2$  is minimized changes in a continuous manner even if  $L_i$  changes sign since  $\chi_i^2 = \chi_{0i}^2$  at  $L_i = 0$ .)

The value of  $\chi_S^2$  is recalculated as track G is rotated (about the pivot at the IP) incrementally in ever decreasing angular steps  $\delta\theta$  and  $\delta\phi$  until the minimum is found within the required precision ( $< 0.1$  mrad, i.e. within  $1\mu\text{m}$  at  $1\text{ cm}$  from the IP). The width of track G is set such that the maximum  $\chi_i^2 = 1.0$  for all tracks with  $L_i > 0$  (if this is less than  $25\mu\text{m}$ , it is restored to  $25\mu\text{m}$ ). The track G is now consistent with all potential  $B$  decay candidate tracks ( $L_i > 0$ ) at the level  $\chi_i^2 \leq 1.0$ . In other words, the new width of G measures the degree to which the tracks conform to a straight line decay chain. A second iteration in  $\delta\theta, \delta\phi$  now takes place with the summed  $\chi^2$  redefined as:

$$\chi_S^2 = \sum_i \begin{cases} \chi_i^2 & L_i \geq 0.0 \\ \chi_{0i}^2 & L_i < 0.0 \end{cases} \quad (14)$$

which is not sensitive to any spurious background track with a negative value of  $L_i$  which might otherwise perturb the direction of track G. After finding the new minimum of  $\chi_S^2$  the width of G is again recalculated such that  $\chi_i^2 \leq 1.0$  for all tracks  $i$  with  $L_i > 0$ . Again this width is required to be at least  $25\mu\text{m}$ . Track G is now directed along the best guess of the  $B$  decay line of flight and has a width such that it is consistent with potential  $B$  decay tracks in the jet, track G is now called the “ghost” track.

The second stage of the algorithm begins by defining a fit probability for a set of tracks to form a vertex with each other and with the ghost track (or IP). This probability then measures the likelihood of the set of tracks both belonging to a common vertex *and* being consistent with the ghost track (or IP) and hence forming a part of the  $B$  decay chain. These probabilities are determined from the fit  $\chi^2$  which is in turn determined algebraically from the parameters of the selected tracks and the ghost track (or the  $7 \times 7 \times 30\mu\text{m}^3$  ellipsoid assumed for the IP). The earlier requirement that each  $L_i > 0$  track makes a  $\chi_i^2 \leq 1.0$  with the ghost track has the effect that the fit probabilities have the desired property of having an approximately flat distribution from 0.0 to 1.0 for genuine

vertices, independent of both multiplicity and decay length. This property also relies on the choice of the number of degrees of freedom as  $2N-2$  (or  $2N$ ) when fitting  $N$  tracks together with the ghost track (or IP). Fake vertices peak at probability close to 0.0.

For a set of  $N$  tracks, there are initially  $N+1$  candidate vertices ( $N$  1-prong secondary vertices and a bare IP). A matrix of track  $i$  – track  $j$  associations is constructed to store the calculated probabilities of each candidate vertex pair fitted together with the ghost track. A further column and row is added to the matrix to store the probabilities of each track fit with the IP ellipsoid. The upper triangle of the matrix (i.e. the  $ij$  ( $i < j$ ) elements) stores the probabilities while the lower triangle (initialized with  $ij$  ( $i > j$ ) elements set to 0.0) indelibly records which tracks (and IP) have been assigned together in a common vertices as the algorithm progresses. Once the upper triangle has been filled, the highest probability in the matrix table is found and the corresponding candidate vertex pair are from then on tied together in a new candidate vertex for all future computations by flagging the corresponding lower triangle elements of the matrix with non-zero values. The upper triangle of the matrix is now refilled taking into account the associations that have so far been made, the new maximum probability is found, and the corresponding subset of the tracks and IP is tied together. At each iteration of combining the maximum probability matrix element contributors, the number of candidate vertices decreases by one. The iterations continue until the maximum probability is less than 1%. At this point the tracks and IP have been divided into unique subsets by the associations thereby defining topological vertices.

Jets or hemispheres in which three vertices are found – the primary (which includes by definition the IP), a secondary and a tertiary – are used for the charge dipole analysis. The secondary vertex is identified as the  $B$  decay vertex and the tertiary as the cascade charm decay. As well as improving the purity and efficiency of the dipole reconstruction (by requiring the vertices be consistent with a single line of flight) the ghost track algorithm has the additional advantage of allowing the direct reconstruction of 1-prong vertices, including the topology consisting of 1-prong  $B$  and  $D$  decays.

Finally, VXD-only tracks are attached to the  $B$  decay chain to improve the overall charge reconstruction but they are not used in the determination of the  $B$  and  $D$  vertex positions. The attachment criteria rely on variables  $\tilde{T}_i$  and  $\tilde{L}_i$  for each track  $i$ , as defined below. A vertex axis is formed by a straight line joining the IP to a vertex combining both secondary and tertiary tracks. The 3-D distance of closest approach of the track to the vertex axis,  $\tilde{T}_i$ , and the distance from the IP along the vertex axis to this point,  $\tilde{L}_i$ , are calculated. Track  $i$  is attached to the vertex if  $\tilde{T}_i < 0.1$  cm,  $\tilde{L}_i > 0.025$  cm and  $0.25 < \tilde{L}_i/\tilde{L} < 2$  (where  $\tilde{L}$  is the distance between the IP and the combined vertex). An average of 0.2 VXD-only tracks is added per decay, to be compared with an average of 5.0 VXD+CDC tracks per decay (for  $M > 2$  GeV/ $c^2$ ). The VXD-only tracks attached to the  $B$  decay chain are further attached to either the  $B$  or  $D$  vertex according to their longitudinal displacement  $\tilde{L}_i$ : tracks with  $\tilde{L}_i < L_B + 0.5(L_D - L_B)$  are attached to the  $B$  vertex and all others are attached to the  $D$  vertex,  $L_B$  ( $L_D$ ) is the distance between the IP and the  $B$  ( $D$ ) vertex.

## 5.2 Event Selection

Hemispheres containing both a secondary and a tertiary vertex are selected for the charge dipole analysis. Furthermore, the invariant mass computed using all secondary and tertiary vertex tracks is required to be  $M > 2 \text{ GeV}/c^2$  (the computed mass includes a partial correction for missing decay products) and the total track charge  $Q_{tot}$  (from both secondary and tertiary vertices) is required to be zero to enhance the fraction of  $B_s^0$  decays in the sample and to increase the quality of the charge difference reconstruction for neutral  $B$  decays. As mentioned in the previous section, the (secondary) vertex that is closer to the IP is labelled “ $B$ ” and that further away (tertiary) is labelled “ $D$ .” A “charge dipole” is defined as  $\delta Q \equiv D_{BD} \times \text{SIGN}(Q_D - Q_B)$ , where  $D_{BD}$  is the distance between the two vertices and  $Q_B$  ( $Q_D$ ) is the charge of the  $B$  ( $D$ ) vertex. Positive (negative) values of  $\delta Q$  tag  $\overline{B}^0$  ( $B^0$ ) decays. Requirements on the vertices are:  $250 \mu\text{m} < D_{BD} < 1 \text{ cm}$ ,  $D$  vertex mass  $< 2.0 \text{ GeV}/c^2$  (assuming all tracks are pions),  $B$  vertex decay length  $L > 0$ ,  $Q_B \neq Q_D$ , “ghost” track width  $< 300 \mu\text{m}$  and cosine between the straight line connecting the IP and the  $B$  vertex, and the nearest jet axis direction  $< 0.9$ . The decay is rejected if any attached VXD-only track has  $p_\perp > 4 \text{ GeV}/c$ , since in that case the charge is not reliably reconstructed. MC studies indicate that, after these selection cuts, the track assignment to the  $B$  ( $D$ ) vertex is 84% (86%) correct for  $B_s^0$  decays containing one  $D$  meson in the final state, i.e. 84% (86%) of all tracks in the  $B$  ( $D$ ) vertex originate from the decay point of the  $B$  ( $D$ ) meson. For all data and MC events, hemispheres already containing a vertex selected by the lepton+ $D$  or  $D_s$ +track analyses are removed to keep the analyses statistically uncorrelated. The  $udsc$  background is further suppressed by demanding that the event contains either an opposite hemisphere topological vertex with  $M > 2 \text{ GeV}/c^2$  or at least 3 tracks with positive 2-D impact parameter  $> 3\sigma$ . The  $udsc$  fraction is thus reduced to 2.2%.

Applying all the above cuts, a sample of 8556 decays is selected in the 1996-98 data. Figure 8 shows distributions of the  $B$  and  $D$  vertex track multiplicities, as well as the distance and charge difference between  $B$  and  $D$  vertices in the selected sample. Good agreement between data and MC is obtained. A slight discrepancy in the  $D$  vertex track multiplicity is apparent but was determined to have negligible impact on the analysis. Requiring that the total track charge be zero boosts the  $B_s^0$  fraction from its assumed production value of 10.0% to 15.3%. Figure 9 displays the distribution of charge dipole  $\delta Q$  for the data sample and also indicates the separation between  $b$  hadrons containing  $b$  or  $\bar{b}$  quarks in the MC.

The average correct tag probability for the charge dipole tag is 0.76 for selected  $B_s^0$  decays and is parameterized as a function of decay length, as shown in Fig. 10. Furthermore, the correct tag probability depends on the charm content of the decay products. Thus, the correct tag probability is parameterized separately for  $B_d^0$  and  $B_s^0$  decays into five different final states:  $D^0 X$ ,  $D^+ X$ ,  $D_s X$ , charmed hadron  $X$ , and  $D\overline{D}X$  (this last category also incorporates charmonium production, i.e. it includes all  $b \rightarrow c\bar{c}s$  decays). For example, the correct tag probability is 0.88 for  $B_s^0 \rightarrow D_s X$  decays but only 0.53 for  $B_s^0 \rightarrow D\overline{D}X$  decays. The above correct tag probabilities are extracted from the MC simulation and include a multiplicative dilution factor  $S_D = 0.95$ . This factor is conservatively assigned to reproduce the overall fraction of decays tagged as mixed observed in



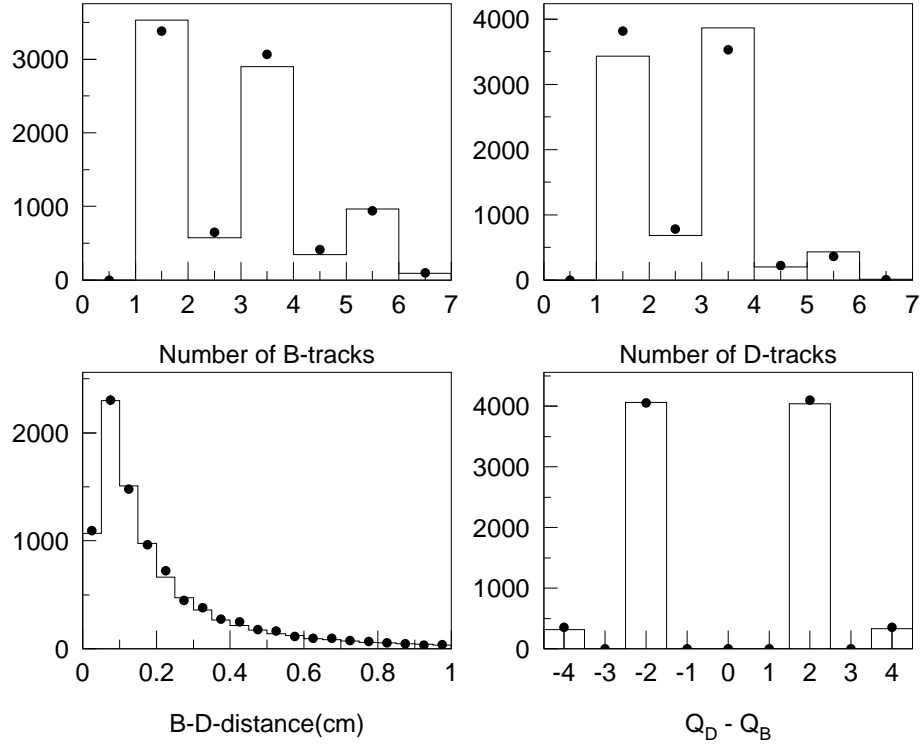


Figure 8: Distributions of  $B$  and  $D$  vertex track multiplicity, as well as distance and charge difference between  $B$  and  $D$  vertices for data (points) and Monte Carlo (histograms) in the charge dipole analysis.

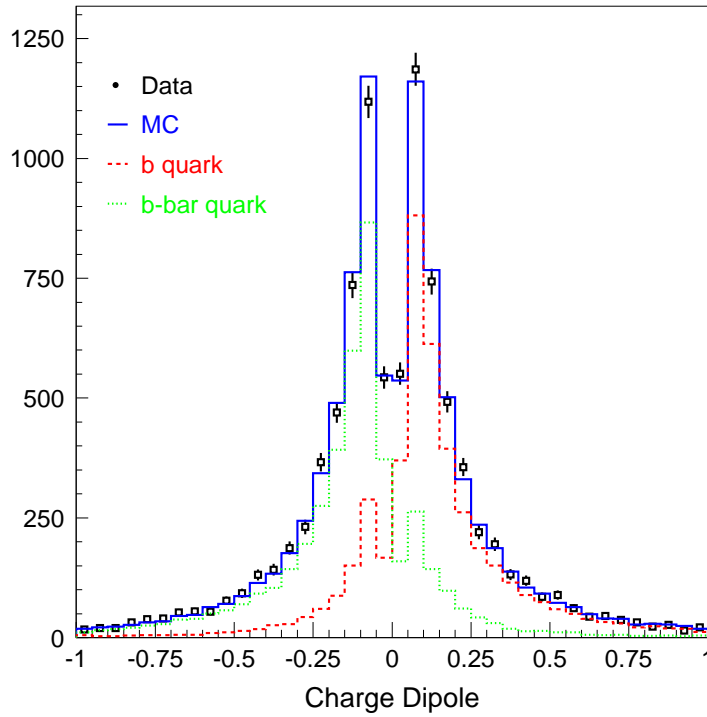


Figure 9: Distribution of the charge dipole for data (points) and Monte Carlo (solid histogram). Also shown are the contributions from  $b$  hadrons containing a  $b$  quark (dotted histogram) or a  $\bar{b}$  quark (dashed histogram).

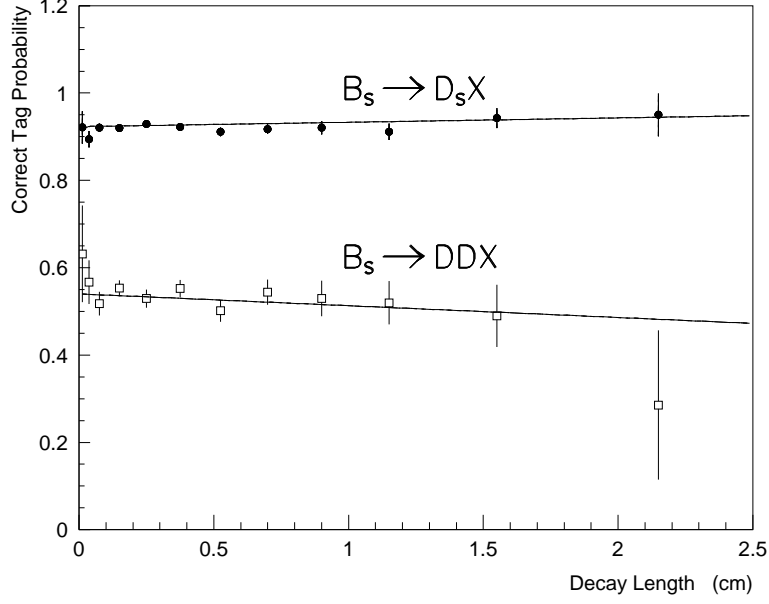


Figure 10: Charge dipole correct tag probability as a function of reconstructed decay length in simulated  $B_s^0 \rightarrow D_s X$  (solid circles) and  $B_s^0 \rightarrow D\bar{D}X$  (open squares) decays. The functions are the fit results used to parametrize the charge dipole correct tag probability as a function of decay length.

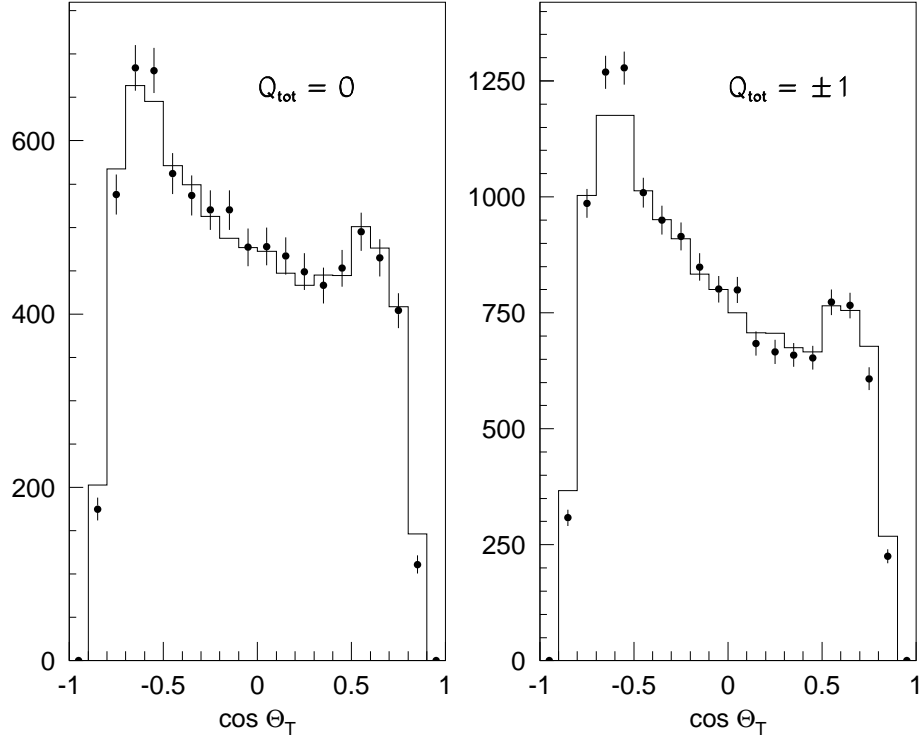


Figure 11: Distributions of  $\cos\theta$  for the thrust axis direction signed by the product  $(\delta Q \times P_e)$  for data (points) and Monte Carlo (histograms) in subsamples with  $Q_{tot} = 0$  and  $Q_{tot} = \pm 1$  for the charge dipole analysis.

the data, as well as to properly describe the time evolution of  $B_d^0-\overline{B}_d^0$  mixing in the data (see below).

As hadronic decays of  $B$  mesons are not as well known as semileptonic decays, it is important to check the correct tag probability estimated using measured quantities like the polarization-dependent forward-backward asymmetry shown in Fig. 11. Good agreement with the MC is observed, indicating that the charge dipole correct tag probability is well modeled. It should be noted that this asymmetry is diluted by both initial and final state mistags and by  $B^0-\overline{B}^0$  mixing. The dilution due to mixing can be reduced by selecting vertices with total charge  $Q_{tot} = \pm 1$ , in which case a stronger asymmetry is observed (see Fig. 11). Another useful test of the charge dipole tag in  $B_d^0$  decays is the measurement of the time dependence of  $B_d^0-\overline{B}_d^0$  mixing. This has been checked using the full likelihood analysis described in the following section. Fitting for the  $B_d^0-\overline{B}_d^0$  mixing frequency yields  $\Delta m_d = 0.495 \pm 0.032 \text{ ps}^{-1}$  (statistical error only), see Fig. 12. This value agrees well with the latest world average value of  $0.485 \pm 0.015 \text{ ps}^{-1}$  [19]. The mixed fraction as a

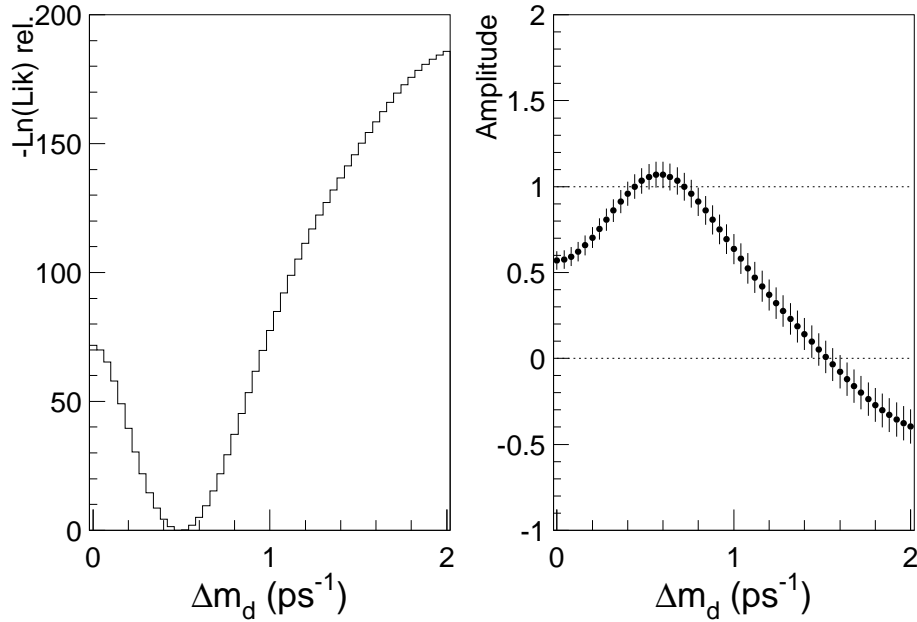


Figure 12: *Log likelihood as a function of  $\Delta m_d$  and measured amplitude as a function of  $\Delta m_d$  for the charge dipole analysis.*

function of proper time is displayed in Fig. 13. The figure shows the expected increase in the fraction of decays tagged as mixed for decays at small proper time. Most of this effect originates from misreconstructed  $B^+$  decays near the IP which tend to have random final state tags.

### 5.3 Likelihood Function

The  $B_s^0-\overline{B}_s^0$  mixing fit for the charge dipole analysis is performed in a way similar to the lepton+D analysis. Decays are tagged as mixed or unmixed if the product  $(P_i - 0.5) \times (P_f - 0.5)$  is smaller or greater than 0, respectively. The probability for a decay to be in

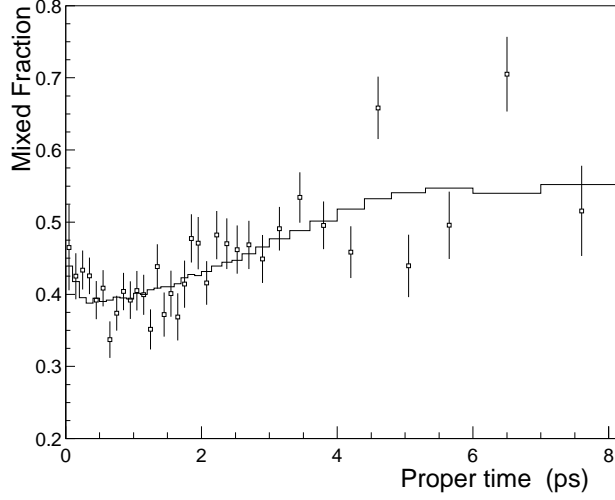


Figure 13: Distributions of the fraction of decays tagged as “mixed” for the data (points) and the likelihood function (histograms) in the charge dipole analysis.

the mixed sample is expressed as:

$$\begin{aligned}
\mathcal{P}_{mixed}(t, \Delta m_s) = & f_u \frac{e^{-t/\tau_u}}{\tau_u} \left[ w^I (1 - w_u^F) + (1 - w^I) w_u^F \right] \\
& + \frac{f_d}{2} \frac{e^{-t/\tau_d}}{\tau_d} \left( \sum_{k=1}^5 g_{dk} \left[ (1 - w_{dk}^F) (1 + [2w^I - 1] \cos \Delta m_d t) + w_{dk}^F (1 - [2w^I - 1] \cos \Delta m_d t) \right] \right) \\
& + \frac{f_s}{2} \frac{e^{-t/\tau_s}}{\tau_s} \left( \sum_{k=1}^5 g_{sk} \left[ (1 - w_{sk}^F) (1 + [2w^I - 1] \cos \Delta m_s t) + w_{sk}^F (1 - [2w^I - 1] \cos \Delta m_s t) \right] \right) \\
& + f_{baryon} \frac{e^{-t/\tau_{baryon}}}{\tau_{baryon}} \left[ w^I (1 - w_{baryon}^F) + (1 - w^I) w_{baryon}^F \right] \\
& + \frac{f_{udsc}}{2} F_{udsc}(t),
\end{aligned} \tag{15}$$

where  $f_j$  represents the fraction of each  $b$ -hadron type and background ( $j = u, d, s, baryon$ , and  $udsc$  correspond to  $B^+$ ,  $B_d^0$ ,  $B_s^0$ ,  $b$ -baryon, and  $udsc$  background),  $F_{udsc}(t)$  is a function describing the proper time distribution of the  $udsc$  background (a sum of two exponentials is used),  $\tau_j$  is the lifetime for  $b$  hadrons of type  $j$ ,  $w^I$  is the initial state mistag probability,  $w_u^F$  and  $w_{baryon}^F$  are the final state mistag probabilities for  $B^+$  and  $b$  baryons, whereas  $w_{dk}^F$  and  $w_{sk}^F$  are the final state mistag probabilities for  $B_d^0$  and  $B_s^0$ , with the index  $k = 1, \dots, 5$  representing the five different decay final states:  $D^0 X$ ,  $D^+ X$ ,  $D_s X$ , charmed hadron  $X$ , and  $D\bar{D}X$ ,  $g_{dk}$  and  $g_{sk}$  are the fractions of  $B_d^0$  and  $B_s^0$  decays into each of the above final states. A similar expression for the probability  $\mathcal{P}_{unmixed}$  to observe a decay tagged as unmixed is obtained by replacing the initial state mistag rate  $w^I$  by  $(1 - w^I)$ .

Several of the quantities in Eq. (15) are determined on an event by event basis. The initial state mistag probability  $w^I$  depends on  $\cos \theta$  of the thrust axis, the electron beam polarization, as well as several quantities from the opposite hemisphere: jet charge, vertex

charge, kaon charge, lepton charge and dipole charge. The final state mistag probabilities  $w_{jk}^F$  depend on the reconstructed decay length to take into account the degradation of the charge dipole tag close to the IP. This effect is fairly weak for  $B_d^0$ ,  $B_s^0$  and  $b$  baryon decays (see, for example, Fig. 10) but it is significant for  $B^+$  decays. Finally, the decay final state fractions  $g_{dk}$  and  $g_{sk}$  are parametrized as a function of the overall vertex mass  $M$ . For example, the fraction of  $B_s^0$  decays into  $D\bar{D}X$  final states decreases from 0.28 at  $M = 2 \text{ GeV}/c^2$  to 0.12 at  $M = 5 \text{ GeV}/c^2$ .

As described in Sec. 4.1, the functions  $\mathcal{P}_{mixed}$  and  $\mathcal{P}_{unmixed}$  are convoluted with a proper time resolution function  $\mathcal{R}(T, t)$ , see Eq. (9) and a time-dependent efficiency function  $\varepsilon_j(t)$ . Separate efficiency functions are extracted for each  $b$  hadron type using the simulation. The relative boost resolution  $\sigma_{\gamma\beta}/\gamma\beta$  is parametrized with the sum of two Gaussians using the MC simulation. Considering all selected  $B_s^0$  decays, the widths of the two Gaussians are  $\sigma_{B1} = 0.07$  and  $\sigma_{B2} = 0.21$ , where the first Gaussian represents 60% of the decays. However, the analysis takes into account the strong dependence of the resolution as a function of total charged track energy in each decay. This is done separately for each of the four different  $b$  hadron types. Offsets in the boost reconstruction, especially for decays with low reconstructed boost, have been corrected for as well.

The decay length resolution is also parametrized by the sum of two Gaussians. For decays with more than 1 track in either the  $B$  or  $D$  vertex, the resolution  $\sigma_L$  is estimated from the  $B$  vertex fit and IP position measurement errors, combined to yield an uncertainty  $\sigma_{meas}$  along the flight direction. The decay length resolution is then obtained by appropriately scaling this quantity to determine a 60% core resolution  $\sigma_{L1} = s_1 \times \sigma_{meas}$  and a 40 % tail resolution  $\sigma_{L2} = s_2 \times \sigma_{meas}$ . For correctly tagged  $B_s^0$  decays we find  $s_1 = 0.92$  and  $s_2 = 2.30$ . For decays with 1 track in each of the  $B$  and  $D$  vertices, the resolution is extracted from the overall decay length residual distributions in the simulation. The difference in decay length resolution between right and wrong charge dipole tags motivates treating those separately in the likelihood function, see Eq. (15). (This is similar to differences in resolution between  $(b \rightarrow l)$  and  $(b \rightarrow c \rightarrow l)$  in the lepton+D analysis.) For example, the average decay length resolution for all  $B_s^0$  decays with right (wrong) charge dipole tag can be parameterized by the sum of two Gaussians of widths  $\sigma_{L1} = 76 \mu\text{m}$  ( $112 \mu\text{m}$ ) and  $\sigma_{L2} = 311 \mu\text{m}$  ( $450 \mu\text{m}$ ), where the first Gaussian represents 60% of the decays. In the case of  $B_d^0$  and  $B_s^0$  decays, the right- and wrong-tag decay length resolutions are estimated for each of the five decay final states. Decays reconstructed within  $200 \mu\text{m}$  of the IP have worse decay length resolution and suffer from asymmetric tails (this is most likely due to the addition of a primary track in the secondary vertex). These effects have been taken into account in the analysis. Finally, offsets in the reconstructed decay length are corrected separately for decays involving one or two charm particles, as the effect is small for the former but not negligible for the latter.

## 5.4 Oscillation Analysis

An amplitude fit is performed, as described in Sec. 4.2 and the result is displayed in Fig. 14. Systematic uncertainties are estimated as for the lepton+D analysis except for those affecting the final state tag. Here, uncertainties in the charge dipole correct tag probability modeling are obtained by varying the scale factor applied to the probability derived from

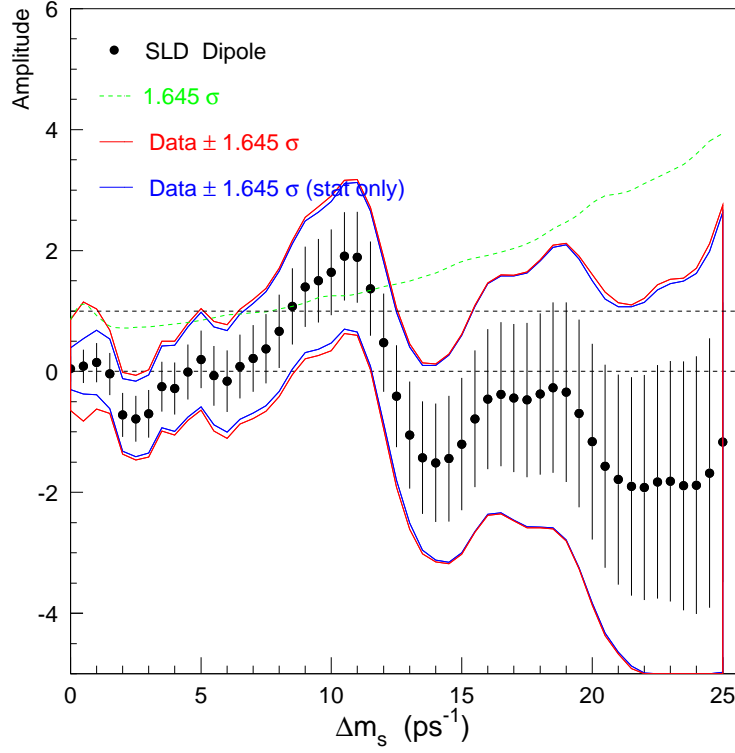


Figure 14: *Measured amplitude as a function of  $\Delta m_s$  in the charge dipole analysis.*

the MC simulation according to  $S_D = 0.95 \pm 0.025$ . In addition, the systematic uncertainty also includes the effect due to a further reduction of the scale factor by 5% for decays within  $L < 0.5$  mm of the IP. Dominant uncertainties are due to the  $B_s^0$  production fraction in  $Z^0 \rightarrow b\bar{b}$  events, the boost and decay length resolutions, and the overall uncertainty in the final state tag purity, see Table 2.

Table 2: Measured values of the oscillation amplitude  $A$  with a breakdown of the main systematic uncertainties for several  $\Delta m_s$  values in the charge dipole analysis.

$\Delta m_s$	5 ps <sup>-1</sup>	10 ps <sup>-1</sup>	15 ps <sup>-1</sup>	20 ps <sup>-1</sup>
Measured amplitude $A$	0.197	1.639	-1.201	-1.162
$\sigma_A^{stat}$	$\pm 0.476$	$\pm 0.711$	$\pm 1.092$	$\pm 1.620$
$\sigma_A^{syst}$	+0.197 -0.178	+0.268 -0.351	+0.159 -0.187	+0.489 -0.189
$f_s = \mathcal{B}(b \rightarrow B_s^0)$	-0.134 +0.172	-0.116 +0.152	-0.105 +0.130	-0.111 +0.116
$f_\Lambda = \mathcal{B}(b \rightarrow b\text{-baryon})$	+0.015 -0.013	+0.020 -0.019	+0.020 -0.020	+0.008 -0.019
$udsc$ fraction	-0.004 +0.004	-0.019 +0.025	-0.025 +0.021	+0.001 +0.004
decay length resolution	+0.017 -0.020	+0.048 -0.035	+0.026 -0.002	+0.080 -0.047
boost resolution	+0.049 -0.044	+0.209 -0.227	+0.075 -0.096	+0.450 -0.084
$B_s^0$ lifetime	+0.039 -0.038	+0.014 -0.017	+0.030 -0.029	+0.028 -0.045
$\Delta m_d$	+0.002 -0.001	+0.001 -0.001	+0.000 -0.002	-0.011 +0.001
initial state tag	+0.001 +0.000	+0.016 -0.014	+0.004 -0.002	-0.106 +0.099
final state tag	+0.069 -0.099	+0.036 -0.236	+0.027 -0.110	+0.074 -0.008

## 6 Combination of the Analyses

The D<sub>s</sub>+tracks, lepton+D and charge dipole analyses are combined taking into account correlated systematic errors. Events shared by two or more analyses are assigned to the analysis with the best sensitivity such as to produce statistically independent analyses. Figure 15 shows the measured amplitude as a function of  $\Delta m_s$  for the combination. As noted earlier, the measured values are consistent with  $A = 0$  for the whole range of  $\Delta m_s$  up to 25 ps<sup>-1</sup> and no evidence is found for a preferred value of the mixing frequency. The following ranges of  $B_s^0\text{-}\overline{B}_s^0$  oscillation frequencies are excluded at 95% C.L.:  $\Delta m_s < 7.6$  ps<sup>-1</sup> and  $11.8 < \Delta m_s < 14.8$  ps<sup>-1</sup>, i.e., the condition  $A + 1.645 \sigma_A < 1$  is satisfied for those values. The combined sensitivity to set a 95% C.L. lower limit is found to be at a  $\Delta m_s$  value of 13.0 ps<sup>-1</sup>. These results are preliminary.

## Acknowledgments

We thank the personnel of the SLAC accelerator department and the technical staffs of our collaborating institutions for their outstanding efforts.

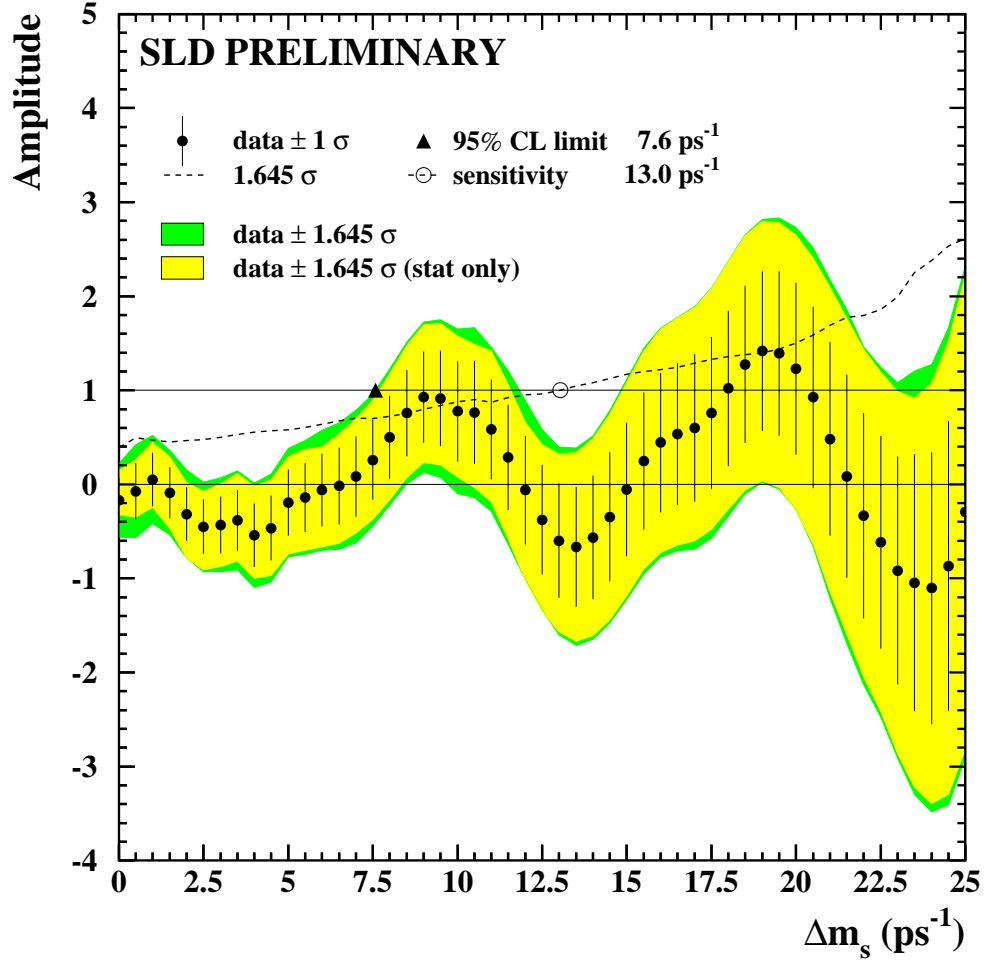


Figure 15: *Measured amplitude as a function of  $\Delta m_s$  for the lepton+D,  $D_s$ +tracks, and charge dipole analyses combined.*



## References

- [1] See the following reviews: F. Caravaglios, F. Parodi, P. Roudeau, and A. Stocchi, *Determination of the CKM unitarity triangle parameters by end 1999*, hep-ph/0002171; S. Mele, Phys. Rev. **D59**, 113011 (1999).
- [2] S. Hashimoto, *B decays on the lattice*, hep-lat/9909136, Nucl.Phys.Proc.Suppl. 83, 3 (2000).
- [3] K. Abe *et al.*, *Time Dependent  $B_s^0 - \overline{B}_s^0$  Oscillations Using Exclusively Reconstructed  $D_s^+$  Decays at SLD*, SLAC-PUB-8598, August 2000.
- [4] K. Abe *et al.*, Phys. Rev. **D53**, 1023 (1996).
- [5] K. Abe *et al.*, Nucl. Inst. and Meth. **A400**, 287 (1997).
- [6] T. Sjöstrand, Comp. Phys. Comm. **82**, 74 (1994).
- [7] CLEO *B* decay model provided by P. Kim and the CLEO Collaboration.
- [8] B. Barish *et al.*, Phys. Rev. Lett. **76**, 1570 (1996); H. Albrecht *et al.*, Z. Phys. **C58**, 191 (1993); H. Albrecht *et al.*, Z. Phys. **C62**, 371 (1994); P. Avery *et al.*, CLEO CONF 96-28, July 1996; L. Gibbons *et al.*, Phys. Rev. **D56**, 3783 (1997); T.E. Coan *et al.*, CLNS 97/1516; CLEO Collab., CLEO CONF 97-27, Aug. 1997; M. Zoeller, Ph.D. Thesis, SUNY Albany, 1994; X. Fu *et al.*, Phys. Rev. Lett. **79**, 3125 (1997); D. Gibaut *et al.*, Phys. Rev. **D53**, 4734 (1996).
- [9] N. Isgur, D. Scora, B. Grinstein, and M.B. Wise, Phys. Rev. **D39**, 799 (1989).
- [10] Particle Data Group, Phys. Rev. **D54**, Part I (1996).
- [11] D. Abbaneo *et al.* (LEP Heavy Flavor Steering Group), *Combined Results on  $b$  Hadron Production Rates, Lifetimes, Oscillations and Semileptonic Decays*, CERN-EP-2000-096, SLAC-PUB-8492, March 2000.
- [12] C. Peterson *et al.*, Phys. Rev. **D27**, 105 (1983).
- [13] R. Brun *et al.*, Report No. CERN-DD/EE/84-1, 1989.
- [14] D. J. Jackson, Nucl. Inst. and Meth. **A388**, 247 (1997).
- [15] K. Abe *et al.* (SLD Collaboration), *Measurement of the  $B^+$  and  $B^0$  Lifetimes using Topological Vertexing at SLD*, SLAC-PUB-8206, July 1999, contributed paper # 477 to EPS-HEP99.
- [16] K. Abe *et al.*, Phys. Rev. Lett. **80**, 660 (1998).
- [17] K. Abe *et al.*, Phys. Rev. **D56**, 5310 (1997).
- [18] H.-G. Moser and A. Roussarie, Nucl. Inst. and Meth. **A384**, 491 (1997).
- [19] See A. Golutvin, *Heavy Flavour Physics*, summary talk presented at ICHEP 2000.

## \*\* List of Authors

Kenji Abe,<sup>(15)</sup> Koya Abe,<sup>(24)</sup> T. Abe,<sup>(21)</sup> I. Adam,<sup>(21)</sup> H. Akimoto,<sup>(21)</sup> D. Aston,<sup>(21)</sup>  
 K.G. Baird,<sup>(11)</sup> C. Baltay,<sup>(30)</sup> H.R. Band,<sup>(29)</sup> T.L. Barklow,<sup>(21)</sup> J.M. Bauer,<sup>(12)</sup>  
 G. Bellodi,<sup>(17)</sup> R. Berger,<sup>(21)</sup> G. Blaylock,<sup>(11)</sup> J.R. Bogart,<sup>(21)</sup> G.R. Bower,<sup>(21)</sup>  
 J.E. Brau,<sup>(16)</sup> M. Breidenbach,<sup>(21)</sup> W.M. Bugg,<sup>(23)</sup> D. Burke,<sup>(21)</sup> T.H. Burnett,<sup>(28)</sup>  
 P.N. Burrows,<sup>(17)</sup> A. Calcaterra,<sup>(8)</sup> R. Cassell,<sup>(21)</sup> A. Chou,<sup>(21)</sup> H.O. Cohn,<sup>(23)</sup>  
 J.A. Coller,<sup>(4)</sup> M.R. Convery,<sup>(21)</sup> V. Cook,<sup>(28)</sup> R.F. Cowan,<sup>(13)</sup> G. Crawford,<sup>(21)</sup>  
 C.J.S. Damerell,<sup>(19)</sup> M. Daoudi,<sup>(21)</sup> S. Dasu,<sup>(29)</sup> N. de Groot,<sup>(2)</sup> R. de Sangro,<sup>(8)</sup>  
 D.N. Dong,<sup>(13)</sup> M. Doser,<sup>(21)</sup> R. Dubois,<sup>(21)</sup> I. Erofeeva,<sup>(14)</sup> V. Eschenburg,<sup>(12)</sup>  
 S. Fahey,<sup>(5)</sup> D. Falciari,<sup>(8)</sup> J.P. Fernandez,<sup>(26)</sup> K. Flood,<sup>(11)</sup> R. Frey,<sup>(16)</sup> E.L. Hart,<sup>(23)</sup>  
 K. Hasuko,<sup>(24)</sup> S.S. Hertzbach,<sup>(11)</sup> M.E. Huffer,<sup>(21)</sup> X. Huynh,<sup>(21)</sup> M. Iwasaki,<sup>(16)</sup>  
 D.J. Jackson,<sup>(19)</sup> P. Jacques,<sup>(20)</sup> J.A. Jaros,<sup>(21)</sup> Z.Y. Jiang,<sup>(21)</sup> A.S. Johnson,<sup>(21)</sup>  
 J.R. Johnson,<sup>(29)</sup> R. Kajikawa,<sup>(15)</sup> M. Kalelkar,<sup>(20)</sup> H.J. Kang,<sup>(20)</sup> R.R. Kofler,<sup>(11)</sup>  
 R.S. Kroeger,<sup>(12)</sup> M. Langston,<sup>(16)</sup> D.W.G. Leith,<sup>(21)</sup> V. Lia,<sup>(13)</sup> C. Lin,<sup>(11)</sup>  
 G. Mancinelli,<sup>(20)</sup> S. Manly,<sup>(30)</sup> G. Mantovani,<sup>(18)</sup> T.W. Markiewicz,<sup>(21)</sup>  
 T. Maruyama,<sup>(21)</sup> A.K. McKemey,<sup>(3)</sup> R. Messner,<sup>(21)</sup> K.C. Moffeit,<sup>(21)</sup> T.B. Moore,<sup>(30)</sup>  
 M. Morii,<sup>(21)</sup> D. Muller,<sup>(21)</sup> V. Murzin,<sup>(14)</sup> S. Narita,<sup>(24)</sup> U. Nauenberg,<sup>(5)</sup> H. Neal,<sup>(30)</sup>  
 G. Nesom,<sup>(17)</sup> N. Oishi,<sup>(15)</sup> D. Onoprienko,<sup>(23)</sup> L.S. Osborne,<sup>(13)</sup> R.S. Panvini,<sup>(27)</sup>  
 C.H. Park,<sup>(22)</sup> I. Peruzzi,<sup>(8)</sup> M. Piccolo,<sup>(8)</sup> L. Piemontese,<sup>(7)</sup> R.J. Plano,<sup>(20)</sup>  
 R. Prepost,<sup>(29)</sup> C.Y. Prescott,<sup>(21)</sup> B.N. Ratcliff,<sup>(21)</sup> J. Reidy,<sup>(12)</sup> P.L. Reinertsen,<sup>(26)</sup>  
 L.S. Rochester,<sup>(21)</sup> P.C. Rowson,<sup>(21)</sup> J.J. Russell,<sup>(21)</sup> O.H. Saxton,<sup>(21)</sup> T. Schalk,<sup>(26)</sup>  
 B.A. Schumm,<sup>(26)</sup> J. Schwiening,<sup>(21)</sup> V.V. Serbo,<sup>(21)</sup> G. Shapiro,<sup>(10)</sup> N.B. Sinev,<sup>(16)</sup>  
 J.A. Snyder,<sup>(30)</sup> H. Staengle,<sup>(6)</sup> A. Stahl,<sup>(21)</sup> P. Stamer,<sup>(20)</sup> H. Steiner,<sup>(10)</sup> D. Su,<sup>(21)</sup>  
 F. Suekane,<sup>(24)</sup> A. Sugiyama,<sup>(15)</sup> S. Suzuki,<sup>(15)</sup> M. Swartz,<sup>(9)</sup> F.E. Taylor,<sup>(13)</sup> J. Thom,<sup>(21)</sup>  
 E. Torrence,<sup>(13)</sup> T. Usher,<sup>(21)</sup> J. Va'vra,<sup>(21)</sup> R. Verdier,<sup>(13)</sup> D.L. Wagner,<sup>(5)</sup> A.P. Waite,<sup>(21)</sup>  
 S. Walston,<sup>(16)</sup> A.W. Weidemann,<sup>(23)</sup> E.R. Weiss,<sup>(28)</sup> J.S. Whitaker,<sup>(4)</sup> S.H. Williams,<sup>(21)</sup>  
 S. Willocq,<sup>(11)</sup> R.J. Wilson,<sup>(6)</sup> W.J. Wisniewski,<sup>(21)</sup> J.L. Wittlin,<sup>(11)</sup> M. Woods,<sup>(21)</sup>  
 T.R. Wright,<sup>(29)</sup> R.K. Yamamoto,<sup>(13)</sup> J. Yashima,<sup>(24)</sup> S.J. Yellin,<sup>(25)</sup> C.C. Young,<sup>(21)</sup>  
 H. Yuta.<sup>(1)</sup>

*(The SLD Collaboration)*

- <sup>(1)</sup> *Aomori University, Aomori , 030 Japan,*
- <sup>(2)</sup> *University of Bristol, Bristol, United Kingdom,*
- <sup>(3)</sup> *Brunel University, Uxbridge, Middlesex, UB8 3PH United Kingdom,*
- <sup>(4)</sup> *Boston University, Boston, Massachusetts 02215,*
- <sup>(5)</sup> *University of Colorado, Boulder, Colorado 80309,*
- <sup>(6)</sup> *Colorado State University, Ft. Collins, Colorado 80523,*
- <sup>(7)</sup> *INFN Sezione di Ferrara and Universita di Ferrara, I-44100 Ferrara, Italy,*
- <sup>(8)</sup> *INFN Lab. Nazionali di Frascati, I-00044 Frascati, Italy,*
- <sup>(9)</sup> *Johns Hopkins University, Baltimore, Maryland 21218-2686,*
- <sup>(10)</sup> *Lawrence Berkeley Laboratory, University of California, Berkeley, California 94720,*
- <sup>(11)</sup> *University of Massachusetts, Amherst, Massachusetts 01003,*
- <sup>(12)</sup> *University of Mississippi, University, Mississippi 38677,*
- <sup>(13)</sup> *Massachusetts Institute of Technology, Cambridge, Massachusetts 02139,*
- <sup>(14)</sup> *Institute of Nuclear Physics, Moscow State University, 119899, Moscow Russia,*
- <sup>(15)</sup> *Nagoya University, Chikusa-ku, Nagoya, 464 Japan,*

- (16) *University of Oregon, Eugene, Oregon 97403,*
- (17) *Oxford University, Oxford, OX1 3RH, United Kingdom,*
- (18) *INFN Sezione di Perugia and Università di Perugia, I-06100 Perugia, Italy,*
- (19) *Rutherford Appleton Laboratory, Chilton, Didcot, Oxon OX11 0QX United Kingdom,*
- (20) *Rutgers University, Piscataway, New Jersey 08855,*
- (21) *Stanford Linear Accelerator Center, Stanford University, Stanford, California 94309,*
- (22) *Soongsil University, Seoul, Korea 156-743,*
- (23) *University of Tennessee, Knoxville, Tennessee 37996,*
- (24) *Tohoku University, Sendai 980, Japan,*
- (25) *University of California at Santa Barbara, Santa Barbara, California 93106,*
- (26) *University of California at Santa Cruz, Santa Cruz, California 95064,*
- (27) *Vanderbilt University, Nashville, Tennessee 37235,*
- (28) *University of Washington, Seattle, Washington 98105,*
- (29) *University of Wisconsin, Madison, Wisconsin 53706,*
- (30) *Yale University, New Haven, Connecticut 06511.*